Lithos 376–377 (2020) 105780

Contents lists available at ScienceDirect

Lithos

journal homepage: www.elsevier.com/locate/lithos

Research Article

Crystal-mush reactivation by magma recharge: Evidence from the Campanian Ignimbrite activity, Campi Flegrei volcanic field, Italy

Sara Di Salvo [a,*], Riccardo Avanzinelli [a], Roberto Isaia [b], Alberto Zanetti [c], Tim Druitt [d], Lorella Francalanci [a,*]

[a] Dipartimento di Scienze della Terra, Università degli Studi di Firenze, Firenze, Italy
[b] Istituto Nazionale di Geofisica e Vulcanologia, Osservatorio Vesuviano, Napoli, Italy
[c] CNR-IGG sezione di Pavia, Italy
[d] Laboratoire Magma et Volcans, OPG-Universitè Clermont Auvergne, Clermont Ferrand, France

ARTICLE INFO

Article history:
Received 15 May 2020
Received in revised form 11 September 2020
Accepted 12 September 2020
Available online 17 September 2020

Keywords:
Crystal-mush reactivation
Micro-analyses
Isotope data
Magma mixing
Campanian Ignimbrite
Campi Flegrei

ABSTRACT

Processes of crystal-mush remobilization by mafic magma recharges are often related to the outpouring of large volumes of silicic melt during caldera-forming eruptions. This occurred for the Campanian Ignimbrite (CI) eruption (Campi Flegrei, Italy), which produced a voluminous trachy-phonolitic ignimbrite in southern-central Italy about 40 ka ago. We focussed on the proximal-CI deposits at San Martino that are composed of a main sequence of early-erupted, crystal-poor units and a late-erupted (post-caldera collapse) crystal-rich Upper Pumice Flow Unit (UPFU). Detailed micro-analytical geochemical data were performed on glasses and crystals of pyroclasts from these deposits and coupled with Sr-Nd isotopic measurements on glasses. Results show that the CI eruption was fed by two distinct melts for the early-erupted units and the late UPFU, respectively. The glasses of the early-erupted units have negative Eu anomalies and show more evolved compositions and higher Nd isotope ratios than those of the UPFU, which have positive Eu/Eu*. The magmas of the early units formed the main volume of eruptible melt of the CI reservoir, and are interpreted as having been extracted from cumulate crystal-mush without a vertical geochemical gradient within the magma reservoir. The data indicate that the generation of the distinctive UPFU melts involved the injection of a new batch of mafic magma into the base of the CI reservoir. The mafic magma allowed heating and reactivation of the CI crystal-mush by melting of low-Or sanidines (+/− low-An plagioclases), leaving high-An plagioclases and high-Mg# clinopyroxenes as residual phases and a crystal-mush melt, made of 20% of the initial mush interstitial melt (with a composition similar to the early-erupted units) and 80% of sanidine melt. When the mush crystallinity was sufficiently reduced, the mafic magma was able to penetrate into the reactivated crystal-mush, mixing with variable proportions of crystal-mush melt and generating cooler hybrid melts, which underwent further crystallization of high-Or sanidine at variable degrees (10–25%). Finally, possibly a short time before the eruption, the UPFU magmas were able to mix and mingle with the crystal-poor eruptible melts still persisting in the CI reservoir at the time of UPFU emission. We suggest that the complex mechanisms described for the magma evolution feeding the CI eruption may occur whenever a crystal-mush is reactivated by new mafic magma inputs

1. Introduction

One of the most challenging tasks of modern volcanology is to understand the processes leading to the generation of large upper crustal magma reservoirs linked to highly explosive eruptions. Caldera-forming eruptions are one of the most hazardous natural events on Earth, but the mechanisms and plumbing system geometries producing these cataclysmic events remain unclear. In the last few decades, detailed volcanological and petrologic studies have suggested complex magmatic plumbing system configurations to explain the compositional characteristics of large ignimbrites. Many of these hypotheses suggest that large silicic melt volumes may be generated by efficient extraction from cumulus crystal-mush zones, remobilised by the arrival of hotter and less evolved magmas into the partially crystallized magma chamber (Bachmann, 2010; Bachmann et al., 2014; Bachmann and Bergantz, 2008; Bacon and Druitt, 1988; Cashman et al., 2017; Cashman and Giordano, 2014; Cooper et al., 2012; Foley et al., 2020; Gualda and Ghiorso, 2013; Wolff et al., 2015).

To investigate these processes we focus on proximal deposits of the Campanian Ignimbrite (CI), which is a caldera-forming eruption that occurred 39.8 ka (Giaccio et al., 2017) from the Campi Flegrei volcanic field in Southern Italy. The CI pyroclastic sequence is characterised by

* Corresponding authors.
E-mail addresses: sara.disalvo@unifi.it (S. Di Salvo), lorella.francalanci@unifi.it (L. Francalanci).

https://doi.org/10.1016/j.lithos.2020.105780

geochemical and isotopic variations, and large lithofacies changes in deposits, from proximal to distal outcrops. Proximal deposits display greater stratigraphic complexity and more heterogeneity in magma components than more distal ones, including large variations in magma crystal content. A plumbing system model based on the presence of a resident crystal-mush reservoir has recently been proposed for the CI (Forni et al., 2016). Accordingly, the proximal-CI stratigraphic sequence represents an ideal case study for understanding the processes leading to crystal-mush reactivation and caldera-forming eruption.

Previous work on the CI has focused mainly on bulk-rock geochemical and isotopic compositions of distal deposits (Civetta et al., 1997). The few papers investigating the proximal-CI outcrops (Fedele et al., 2008; Melluso et al., 1995) are mostly based on whole-rock data and do not report isotopic ratios. Less abundant data on glasses, which are representative of the eruptible portions of the magma chamber, are available for the proximal-CI deposits and do not cover all the eruption phases (Fedele et al., 2008; Forni et al., 2016; Marianelli et al., 2006; Smith et al., 2016; Tomlinson et al., 2012).

In order to provide a complete picture of compositional heterogeneity of the CI magmas, we performed geochemical and isotopic microanalyses on interstitial glasses of all the proximal-CI juvenile components, including distinct portions of individual pyroclasts. Feldspar and clinopyroxene mineral chemistries were also determined to better characterise the crystal cargo of the CI. The samples were collected from the pyroclastic sequence at San Martino, within the city of Naples, which is one of the most complete proximal-CI successions and includes one of the best exposures of the topmost crystal-rich stratigraphic unit: the Upper Pumice Flow Unit (UPFU) (Fedele et al., 2008). This final unit is characterised by juvenile clasts with the least evolved glasses, and highest crystal content, of the whole CI sequence. The study investigates in particular the possible role of fresh magma inputs into a crystal-mush zone of a large silicic reservoir prior to its eruption.

2. Volcanological and petrologic background

The Campi Flegrei nested caldera (Fig. 1a) is one of the most historically active volcanic complexes in Europe. It was the site of the 40 ka Campanian Ignimbrite (CI) eruption, one of the largest and most intense eruptions in the Mediterranean area in the last 200 ka (Barberi et al., 1978; Costa et al., 2012; Giaccio et al., 2008, 2017; Marti et al., 2016). The eruptive activity at Campi Flegrei started more than about 80 ka through several explosive eruptions and minor effusive events

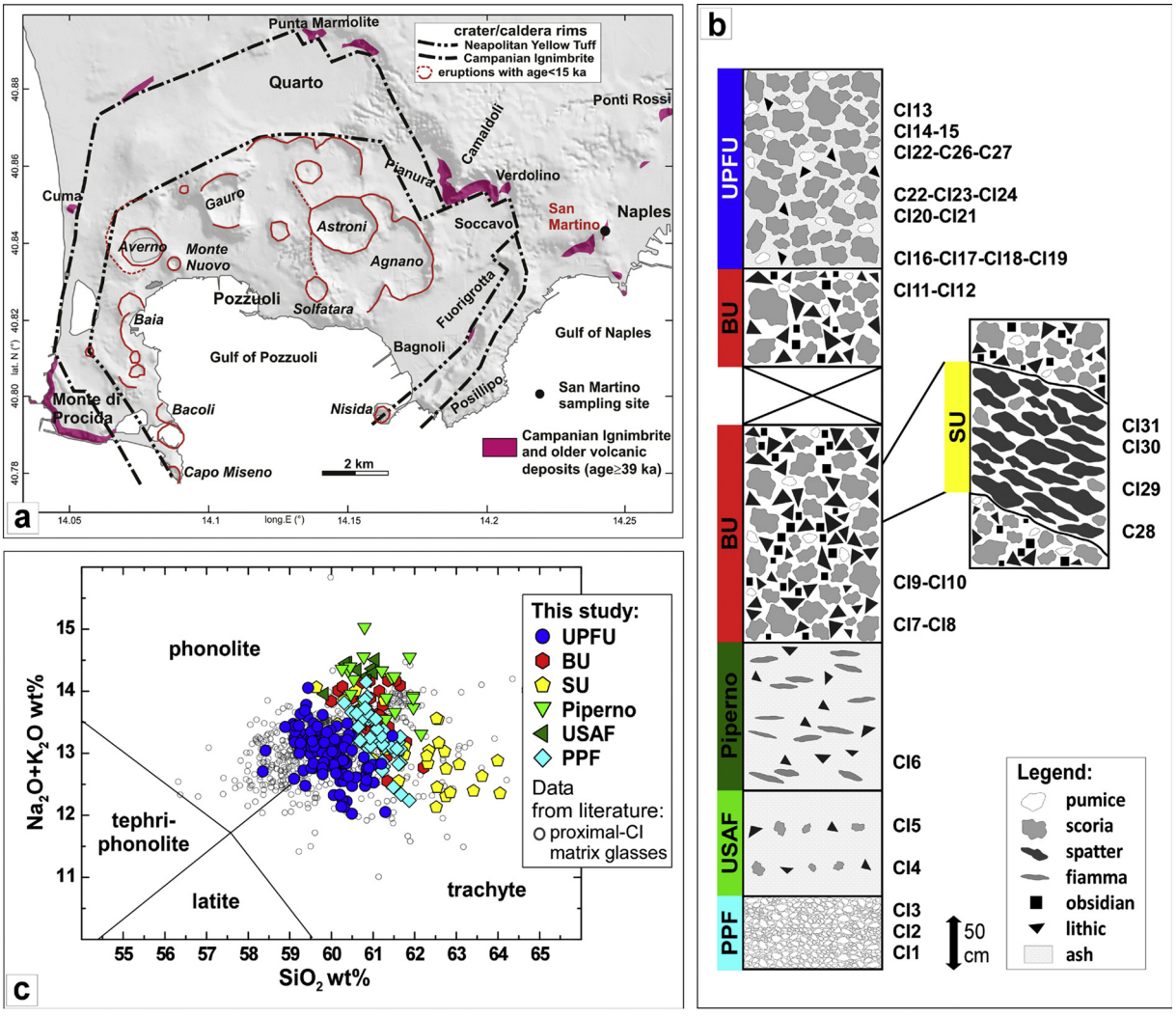

Fig. 1. a) Sketch map of the Campi Flegrei caldera (modified after Vitale and Isaia, 2014) showing the location of the San Martino outcrop and the proximal-CI deposits along and close to the external caldera boundary. b) Stratigraphic sequence of the San Martino outcrop, including five of the six proximal-CI type units reported by Fedele et al., 2008. The cross marks a stratigraphic gap within the BU level. The locations of the juvenile samples collected along the sequence are also reported. c) Total alkalis vs silica (TAS; Le Maitre, 1989) classification diagram for the San Martino matrix glasses. Grey symbols represent literature data for the proximal-CI units (Fedele et al., 2008, 2016; Forni et al., 2016; Smith et al., 2016). PPF: Plinian Pumice Fall; USAF: Unconsolidated Stratified Ash Flow; Piperno: Piperno welded tuff; BU: Breccia Unit; SU: Spatter Unit; UPFU: Upper Pumice Flow Unit.

(e.g., Pappalardo et al., 1999). Magma compositions vary from shoshonite to phonolite, with trachyte and phonolite being most abundant (e.g. D'Antonio et al., 1999).

The CI eruption laid down thick pyroclastic deposits up to 80 km from the Campi Flegrei and caused caldera collapse. Ash fallout from the eruption occurred as far away as the eastern Mediterranean Sea and Russia (Fedele et al., 2002; Lowe et al., 2012; Perrotta et al., 2006; Pyle et al., 2006; Smith et al., 2016).

Many studies have described the stratigraphy of the CI deposits, taking into account proximal, medial and distal outcrops (Barberi et al., 1978; Cappelletti et al., 2003; Fedele et al., 2008, 2016; Fisher et al., 1993; Rosi et al., 1996; Scarpati and Perrotta, 2016).

The proximal-CI deposits, also referred to as the "Breccia Museo sequence" (Fedele et al., 2008; Melluso et al., 1995), crop out close to the Campi Flegrei caldera rim (Fig. 1a). Following the description of Fedele et al. (2008), the proximal-CI type-section, from bottom to top (Fig. 1b), is composed of: 1) a moderately to well sorted, stratified and coarse Plinian Pumice Fall deposit (PPF); 2) an Unconsolidated Stratified Ash Flow level (USAF); 3) a highly welded tuff called Piperno, consisting of welded ash beds and flattened scoriae (*fiamme*) and a coarse breccia of lava fragments; a lateral transition to sintered ignimbrite, considered the equivalent of the distal Welded Grey Ignimbrite (WGI), has been suggested (Fedele et al., 2016); 4) the Lower Pumice Flow Unit (LPFU), a poorly sorted and pumice-rich level; 5) a crudely stratified lithic breccia (BU), which also includes juvenile clasts of scoria, pumice and obsidian, and it is interlayered by welded spatter beds (SU); 6) the topmost Upper Pumice Flow Unit (UPFU), consisting in an unconsolidated and poorly sorted level with scoriaceous and pumiceous juvenile clasts; UPFU is also locally found interlayered with the BU/SU deposits. The described stratigraphic sequence derived by different eruptive phases occurred during the CI.

The eruption began with the onset of a Plinian plume associated with the deposition of the basal stratified pumice fallout (PPF). The column collapse generated large pyroclastic density currents, spreading over an area of 30,000 km^2 (Fisher et al., 1993; Scarpati et al., 2014) and outpouring the CI intermediate units of the sequence (Piperno/WGI and LPFU). The main caldera collapse event likely occurred in the late phase of the CI activity, after deposition of the main ignimbrite and during the emission of BU (Fedele et al., 2008; Rosi et al., 1996), as suggested by the abundant amounts of different lithic fragments in the BU (Fedele et al., 2009; Gebauer et al., 2014). The topmost UPFU of the proximal-CI sequence was emplaced immediately after caldera collapse.

Published whole-rock and matrix glasses from the CI eruption straddle the boundary between trachyte and phonolite, with the least evolved compositions found in the last erupted, crystal-rich units (UPFU and partially BU/SU) (Fedele et al., 2008; Forni et al., 2016; Smith et al., 2016). These units also generally display lower Sr- and Nd-isotope ratios than the most-evolved ones (Arienzo et al., 2009; Civetta et al., 1997; Pappalardo et al., 1999). Only few $^{87}Sr/^{86}Sr$ and $^{143}Nd/^{144}Nd$ data are available in literature for CI glasses (Arienzo et al., 2011; Civetta et al., 1997; Pappalardo et al., 2002a), with ranges of 0.70723–0.70747 and 0.51248–0.51251, respectively.

Some authors ascribe the geochemical variations in the CI sequence to closed-system magma evolution by fractional crystallization, representing a classically zoned magma reservoir from which a progressively less evolved magma is tapped (Fedele et al., 2008; Fowler et al., 2007). Other studies have suggested the occurrence of open-system evolutionary processes where the less evolved magmas represent new magma inputs that are not co-genetic with the more evolved resident magmas (Arienzo et al., 2009; Civetta et al., 1997; Pappalardo et al., 2002a; Signorelli et al., 1999). Recently, a detailed mineralogical study by Forni et al. (2016) provided a more complex picture for the CI magmatic system, suggesting the presence of a crystal-mush zone where a crystal-poor evolved melt is extracted during the formation of cumulates, creating a buoyant cap at the top of the chamber. The trigger for the eruption was attributed to recharge of hotter mafic magma at the base of the reservoir that released heat to the mush allowing crystals to be partially melted. In this view, the mafic input makes minimal mass contribution to the erupted magmas, preferentially acting as a thermal trigger for cumulate melting.

3. Material and methods

3.1. Sample collection and preparation

Analyses were performed on matrix glass (hereafter referred simply as 'glass') and minerals of pyroclasts from the proximal-CI sequence of San Martino, located north-west of Naples (40°84′23.53″, 14°24′24.04″) (Fig. 1a,b). The stratigraphy was studied by Rolandi et al. (2003) and partially geochemically investigated by Fedele et al. (2008) and Smith et al. (2016). This outcrop displays one of the most complete proximal-CI stratigraphic sequences, showing five (PPF, USAF, Piperno, BU/SU and UPFU) of the total six units. The location along the sequence of the 31 samples collected (CI1-CI31) is reported in Fig. 1b and complete outcrop and sample descriptions are provided as Supplementary Material (S.M.1) and in the Supplementary Table 1.

Selected single pyroclasts were cleaned in repeated ultrasonic baths and cut into two portions to get two corresponding slices from the same clast, one to perform the polish sections for petrographic observations and micro-analyses on glasses and minerals, the other for Sr- and Nd-isotope data performed on hand-picked glasses (Fig. S.1 of Supplementary Material). Different glass zones inside a single clast (or polished section area) were investigated. In this way, we were able to couple in-situ major and trace element data with isotopic measurements of different zones in each clast (Figs. S.1, S.2 of the Supplementary Material). A complete description of the sample preparation is provided as Supplementary Material (S.M.2).

3.2. Analytical methods

Major element compositions of matrix glasses and minerals were determined at CNR-IGG of Florence, using a microprobe JEOL-JXA 8600. Few samples were analysed at the Laboratoire de Magma et Volcans, Université Clermont-Auvergne, Clermont Ferrand (France) with a CAMECA SX100 microprobe. Operation conditions for both instruments were 15 kV and a beam diameter of 5–15 μm; beam currents were 10 nA and 4 nA for the analyses performed in Florence and Clermont Ferrand, respectively. Replicate analyses of international standards measured on both instruments are reported in the Supplementary Tables 2,3.

Trace element compositions of mineral phases and matrix glass were measured by LA-ICPMS in two laboratories: a) at the CNR-IGG of Pavia, using a quadrupole ICP-MS system (DRCe from PerkinElmer) connected to a NWR213 laser ablation system from New Wave Research; b) at the Laboratoire Magma et Volcans de l'Observatoire de Physique du Globe in Clermont-Ferrand (France) through a quadrupole ICP-MS Agilent 7500 system connected to a 193 nm Resonetics M-50E laser system with the ultra-short (<4 ns) ATL laser. Accuracy and precision for both instruments were verified through replicate measurements of international standards BCR-2G (provided in Supplementary Table 4). For both instruments, long-term laboratory reproducibility of glass standards indicates precision significantly better than 5% for elements whose concentration was greater (i.e. 2×) than the detection limit.

Sr and Nd isotope measurements were performed at the Radiogenic Isotope Laboratory of the Department of Earth Sciences, University of Florence. Isotope ratios were determined with a Thermal Ionization Mass Spectrometer (TIMS: ThermoFinningan™ Triton TI™) in multi-dynamic mode following the analytical procedure described in Avanzinelli et al. (2005). Hand-picked glasses were leached before chemical digestion to avoid any possible contribution from alteration

(a complete description of the leaching is reported in the Supplementary Material S.M.3). Long-term reproducibility on NIST SRM987 and La Jolla standards yielded mean values of $^{87}Sr/^{86}Sr = 0.710248 \pm 0.000016$ (2 s, $n = 57$) and $^{143}Nd/^{144}Nd = 0.511846 \pm 0.000007$ (2 s; $n = 67$), respectively, which are identical within error of the reference values (0.710249 ± 0.000011 and 0.511856 ± 0.000007, respectively in Thirlwall, 1991). For Nd isotopes, replicate analyses of an in-house Nd standard (Nd-Fi) were also performed, yielding values of $^{143}Nd/^{144}Nd = 0.511467 \pm 0.000007$ (2σ; $n = 111$). The within run Sr analytical blank was 128 pg, which is in the blank range of the laboratory. The full dataset, including standards, is provided in Supplementary Table 5. All the isotope data were corrected for the age of the deposits (39.8 ka, Giaccio et al., 2017).

Further details on the whole sample preparation and analytical procedures are provided as Supplementary Material (S.M.2, S.M.3).

4. Results

In what follows we distinguish between the chemically evolved units PPF, USAF, Piperno, LPFU and BU/SU (referred to jointly as the 'early-erupted units'), and the less evolved unit UPFU that was discharged at the end of the eruption (Fig. 1b).

4.1. Petrography and mineral chemistry

The CI pyroclasts range from aphyric to highly porphyritic. Crystals of phenocryst size are dominantly sanidine with subordinate plagioclase, clinopyroxene and biotite; magnetite and apatite are accessory phases. Pyroclasts of the early-erupted units generally have low crystal contents (~3–8 vol%), while those of UPFU are more crystal-rich (up to 30–35 vol%). A previous study (Forni et al., 2016) reported the presence of crystal-rich pumices (up to 36 vol%) in the BU, but these pumices were not found in the studied sequence (S. Martino).

Sanidine is the main mineral phase, being most abundant in UPFU, where it reaches 80–90 vol% of the total crystal content and occurs as large (up to 1.5 cm) euhedral crystals. We recognized two sanidine groups with high and low Or contents (Or_{83-88} and Or_{55-72}, respectively; Fig. 2a, Supplementary Table 2). The high-Or group is mainly found in UPFU as large euhedral crystals with limited zoning (both normal and reverse) in terms of major element contents. The low-Or sanidines occur in the early-erupted units; they are also mainly euhedral and display normal zoning and a wider compositional range than the high-Or ones. Rare low-Or sanidines have also been observed in UPFU (Fig. 2a).

Plagioclase has a maximum size of about 0.6–0.8 mm and increases in abundance upwards stratigraphically toward UPFU, where it can represent >10 vol% of the total crystal content. It varies in composition from bytownite (An_{95}) to oligoclase (An_{23}) (Fig. 2b, Supplementary Table 2). Compositions cluster into high-An (An_{78-95}) and low-An (An_{24-41}) groups. Plagioclases of the high-An group are ubiquitous in all the units, whereas the low-An plagioclases are only present in the early-erupted units. Accordingly, only high-An crystals are found in UPFU. High-An plagioclases are often subhedral, non-zoned or with weak normal zoning (Fig. 2b). Contrarily to sanidine, they commonly have sieve textures and partially resorbed shapes. High-An plagioclases from the early-erupted units are often found as cores in crystals with low-An rims (Fig. 2b). The low-An plagioclases occur both as individual homogeneous crystals and as rims over high-An cores, both displaying euhedral shapes.

Clinopyroxenes (maximum size of 500 μm) display a variety of textures, from euhedral shapes to completely resorbed edges, and compositions ranging from Mg# 57 to 91 (Fig. 2c, Supplementary Table 2). UPFU clinopyroxenes clearly display two distinct compositions: diopsidic Mg-rich crystals (Mg# = 82–87) mainly forming cores and Fe-richer components found both as rims of the diopsidic cores (Mg# = 60–67) and as individual homogeneous crystals (Mg# = 57–64) (Fig. 2c). The clinopyroxenes analysed in the early-erupted units display intermediate compositions (Mg# = 66–76), with the exception of a single Mg-rich crystal within PPF (Fig. 2c).

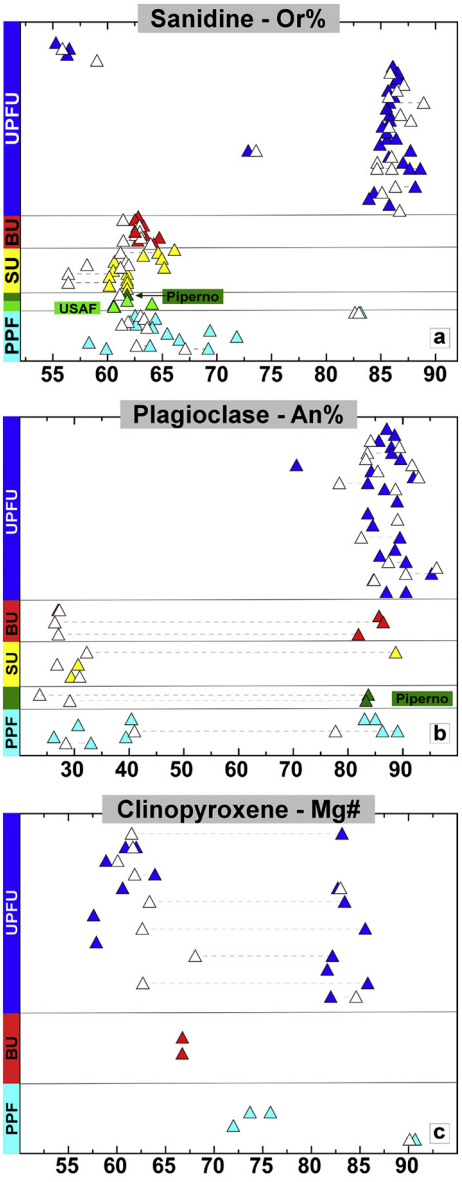

Fig. 2. Compositional variation of sanidine (a), plagioclase (b) and clinopyroxene (c) crystals in the juvenile clasts from San Martino proximal-CI sequence. Symbols aligned at the same height represent different spot of analyses within the same crystal. Full triangles: cores, open triangles: rims. Where wider zoning was displayed inside a single crystal, a dotted grey line connects compositions from core to rim for highlighting heterogeneities.

4.2. Glass compositions

All the glasses from the San Martino outcrop are trachy-phonolites and fit well within the range of literature data (Fig. 1c). Glasses of the early-erupted units are generally more evolved (CaO = 0.17–2.45 wt%, MgO = 0.12–0.44 wt%) (Figs. 1c,3a; Supplementary Tables 3) than those of UPFU (CaO = 1.65–3.33 wt%, MgO = 0.40–1.00 wt%). A few evolved glasses have, however, been also detected in a pumiceous clast of UPFU (Fig. 3a).

The trace element compositions of the glasses reflect those of the major elements. Glasses of the early-erupted units display mutually similar ranges both in compatible (e.g., Ba, Sr, V) and incompatible

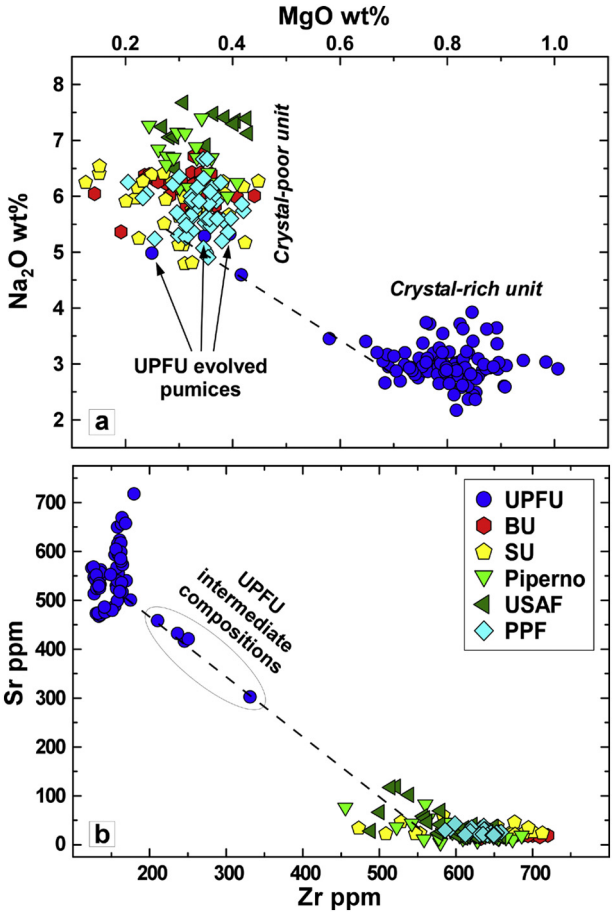

Fig. 3. Major and trace element variation of glasses from the San Martino sequence; a) MgO vs. Na_2O wt%, b) Zr vs. Sr (ppm). UPFU glasses display distinct and less evolved compositions with respect to those of the previously erupted units, having higher MgO and compatible elements (e.g. Sr) and lower Na_2O and incompatible element (e.g., Zr) contents.

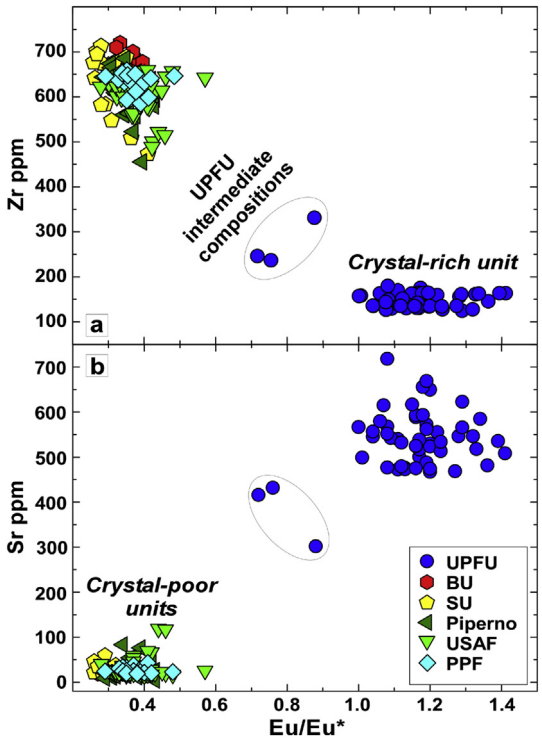

Fig. 4. Eu/Eu* vs. Zr (a) and Sr (b) of glasses from the San Martino sequence.

trace element contents (e.g., Zr, Th, Rb) (Fig. 3b). They have systematically higher contents of incompatible trace elements (Fig. 3b) than the UPFU glasses, while being depleted in compatible ones. The latter show limited variations in the early-erupted units, whilst being more variable in UPFU. Incompatible elements show the opposite behaviour, being rather constant in UPFU and significantly more variable in the early-erupted units. Only a few trace element data points of UPFU are intermediate between the two main glass groups (Fig. 3b, Supplementary Table 4).

The glasses of the early-erupted units display relatively high REE content and negative Eu anomalies ($Eu/Eu^* = 0.12–0.58$), whereas most UPFU glasses have lower REE contents and slightly negative to positive Eu anomalies ($Eu/Eu^* = 0.98–1.4$) (Fig. 4).

Sr- and Nd-isotope ratios were analysed on 38 glasses. $^{87}Sr/^{86}Sr$ values show significant variability (0.70731–0.70746) with no clear distinction between the early-erupted units (PPF, BU/SU) and UPFU (Fig. 5a, Fig. S.2 of Supplementary Material). The measured isotopic range is similar to that of published data on CI glasses (0.70723–0.70747; Fig. 5b), although data from literature are not univocally correlated/referred to single CI units.

$^{143}Nd/^{144}Nd$ values of the glasses of the early-erupted units vary in the range 0.51250–0.51252 (Figs. 5a,7), also within the published range (0.51249–0.51251) (Fig. 5b), with no distinction between different units. UPFU glasses are instead distinct, having lower and more variable $^{143}Nd/^{144}Nd$ (0.51245–0.51249), extending to values less radiogenic than the whole published range of CI (Fig. 5, Fig. S.2 of Supplementary Material). Among UPFU data, the lowest Nd isotope ratios occur in the glasses with high Ba, Sr and V contents (Fig. 6, Supplementary Tables 4,5).

In Fig. 5a, glasses of early-erupted units show slightly higher and more variable $^{87}Sr/^{86}Sr$ than UPFU glasses, with the exception of few UPFU data points with $^{87}Sr/^{86}Sr > 0.70738$. These high $^{87}Sr/^{86}Sr$ UPFU glasses have also relatively high $^{143}Nd/^{144}Nd$ (clasts CI26a, CI27a) and correspond to the few more evolved UPFU pumice glasses reported in Fig. 3a.

It is worth stressing that significant compositional and isotopic variability occurs also within individual pyroclasts and, in some cases, even within the same thin-section (e.g., Fig. S.2 of Supplementary Material), with ranges sometimes as large as in the whole stratigraphic unit (e.g., the SU scoria sample CI29a; Supplementary Tables). In fact, the early-erupted units do no show any compositional gradient with stratigraphy, whilst a significant change occurs only in the UPFU.

5. Discussion

Our data show that magmas and melts of the late-erupted unit UPFU (Figs. 2–5) are different in mineralogical, chemical and isotopic characteristics from those of the rest of the eruption. This is in contrast with previous studies on proximal-CI sequences, which suggested the presence of a broad vertical geochemical gradient linked to a zoned magma chamber (Fedele et al., 2016; Melluso et al., 1995; Pappalardo et al., 2002b). Previous work was mostly based on whole-rock data, which may be not representative of melts present in the system. Literature data on matrix glass of the proximal-CI are limited (Fedele et al., 2008; Smith et al., 2016) and sometimes difficult to relate to the specific stratigraphic units. The detailed work on glass data made in this study, allow us instead to document liquid compositions through the eruption sequence, and to relate them to dynamic processes occurring in the magma reservoir. In this way, two distinct groups of melts feeding the CI eruption can be recognized: one erupted first as the early-erupted units (PPF-USAF-Piperno-BU/SU), and the other erupted later within

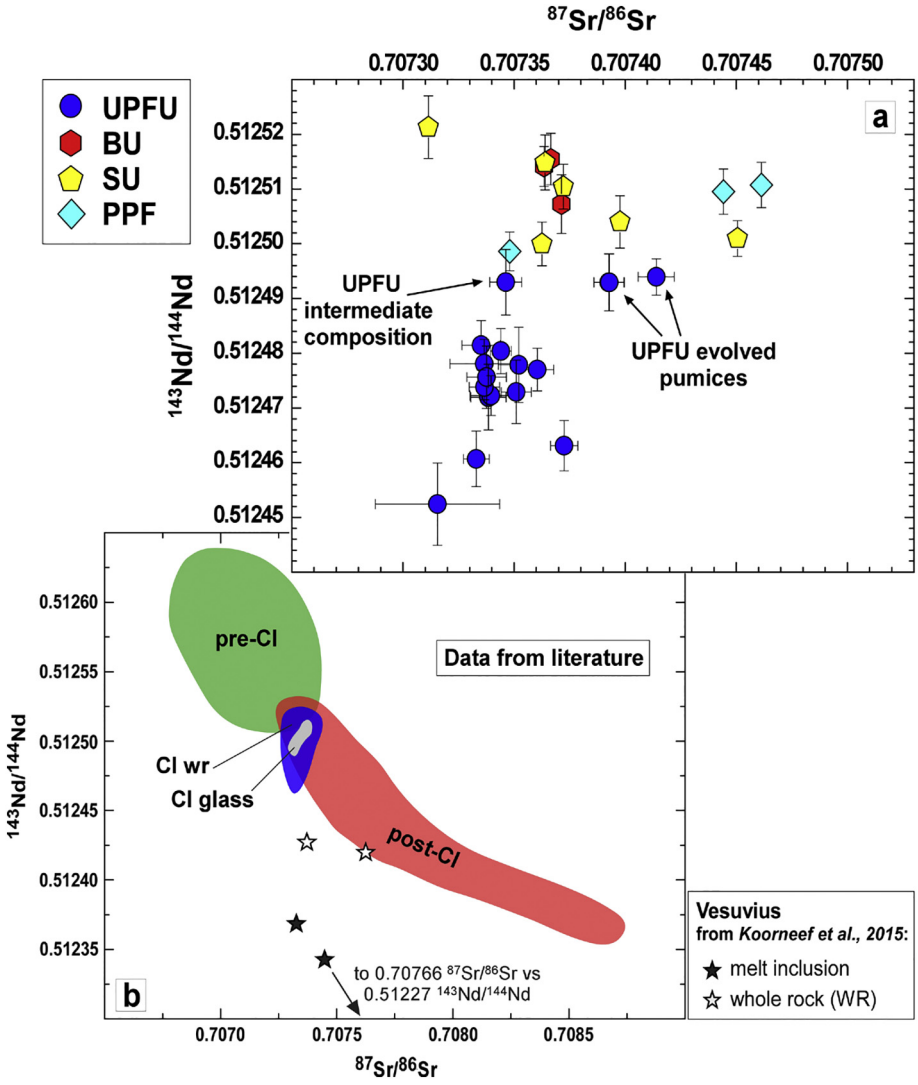

Fig. 5. a) $^{87}Sr/^{86}Sr$ vs. $^{143}Nd/^{144}Nd$ of glasses from the San Martino sequence. b) Sr vs. Nd isotope variations of the Campi Flegrei whole-rocks (wr), divided in the pre-CI, CI and Post-CI periods and based on literature data (data sources: Civetta et al., 1991; Orsi et al., 1992; Pappalardo et al., 2002a, 2002b; D'Antonio et al., 2007; Pabst et al., 2008; Tonarini et al., 2009; Arienzo et al., 2009; Di Renzo et al., 2011; Di Vito et al., 2011). The grey field refers to the few data available for CI matrix glasses (Arienzo et al., 2009; Civetta et al., 1997; Di Renzo et al., 2011).

the late stage UPFU unit (Fig. 1b). The same compositional variability in CI-proximal glasses was reported by two previous studies (Smith et al., 2016; Tomlinson et al., 2012).

The melts of the early-erupted units are more evolved (Figs.3,4) and have higher Nd-isotope ratios (Figs.5a,6) than those of UPFU. They also show negative Eu/Eu* values (Fig. 4), testifying to abundant feldspar

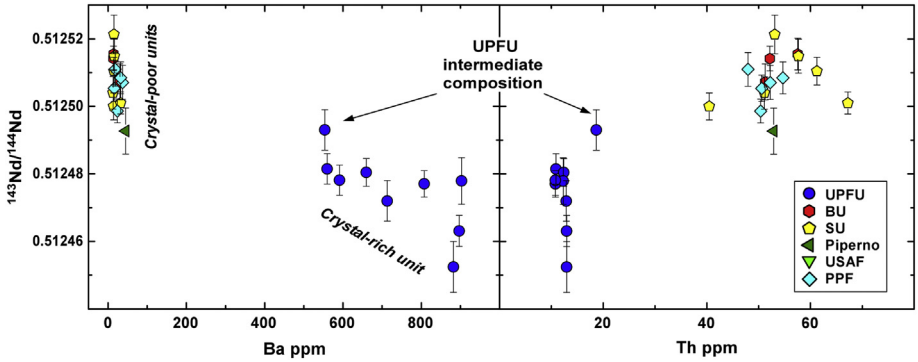

Fig. 6. Nd isotopes vs. compatible (e.g., Ba) and incompatible (e.g., Th) trace elements within glasses from the San Martino sequence.

fractionation. The melts feeding UPFU have instead generally positive Eu anomalies (Fig. 4).

The dichotomy observed in the glasses is also found in the petrography and mineral chemistry. The crystal-rich UPFU melts are in equilibrium with euhedral high-Or sanidine (Fig. 2), whilst low-Or sanidine (along with low-An plagioclase and low-Mg clinopyroxene) is the stable phase in the early-erupted units. This is consistent with a higher temperature for UPFU magmas (970–1050 °C) than for those of the more evolved, crystal-poor units (900–950 °C; Forni et al., 2016).

5.1. The crystal-poor, more evolved magmas of the Campanian Ignimbrite

The highly evolved trachy-phonolitic composition and low crystal contents of the magmas of the early-erupted units suggest derivation by melt extraction from cumulate crystal mushes. This process has been proposed for many large silicic magma chambers (e.g., Bachmann and Huber, 2016) including the Campi Flegrei system (Forni et al., 2016; Voloschina et al., 2018). In this model, buoyant crystal-poor evolved melts are extracted from the crystal-mush, accumulating to build the eruptible magma portion of the reservoir. The crystal-mush is a quasi-rigid crystalline skeleton containing a high amount of minerals (>60%, Marsh, 1981; Bachmann and Bergantz, 2008) together with silicic interstitial melts similar in composition to, or possibly more evolved than, the crystal-poor extracted melts.

Glasses of the early-erupted units display a large variability. In some cases, extremely different glass compositions were found at the micro-scale within the same pyroclast, showing the presence of chemical heterogeneity in the more evolved melts co-extracted during the eruption. A more detailed study of this small-scale heterogeneity will be described in a future paper. The aim of the present study is to constrain the origin of the magmas feeding the final phase of the eruption, represented by the UPFU glasses.

5.2. The crystal-rich, less evolved magmas of the Campanian Ignimbrite

The UPFU has mineralogical (Fig. 2), geochemical (Figs.3,4) and isotopic (Figs. 5,6) characteristics clearly different from those of the early-erupted units. They show particularly low incompatible element contents (e.g., Th, Zr) even when compared to other Campi Flegrei magmas of similar evolutionary degree (Fig. 7). We propose that this requires the involvement of: i) a new mafic magma input, ii) at least two crystal-mush components (melts of cumulate crystals and interstitial-melts) and iii) crystal fractionation.

5.2.1. Evidence for the contribution of a new mafic magma

One of the most distinctive characteristics of the UPFU glasses is their Nd-isotope signature (Fig. 5). Compared to the $^{143}Nd/^{144}Nd$ values of the more evolved CI glasses, those of UPFU glasses are lower and more variable. This suggests that less evolved and isotopically distinct new melts were directly involved in the origin of the UPFU magmas and thus might have contributed with mass addition more than previously hypothesised by Forni et al. (2016). These melts must have entered the resident CI system hosting the highly evolved melts (represented by the early-erupted units) and the related crystal-mush. Field, stratigraphic and volcanological evidence support this hypothesis, indicating that the UPFU was emplaced immediately after and sometimes even interlayered with, the BU/SU deposits (e.g., Fedele et al., 2008, 2016; Scarpati and Perrotta, 2016). This implies that the two different melt types had to be present in the same reservoir at the time of eruption.

In order to investigate the geochemical and isotopic variability of UPFU glasses, it is necessary to constrain the Nd-isotope signature of the fresh magma entering into the CI reservoir. The broad increase of $^{143}Nd/^{144}Nd$ at decreasing compatible element contents in the UPFU glasses (Fig. 6) suggests that the new magma was characterised by low Nd-isotopes, possibly similar to the lowest value found in our dataset (Supplementary Table 6), as well as rather low Sr-isotopes. The other UPFU glasses must reflect a differentiation process able to increase the $^{143}Nd/^{144}Nd$, without significantly changing $^{87}Sr/^{86}Sr$ (Fig. 5).

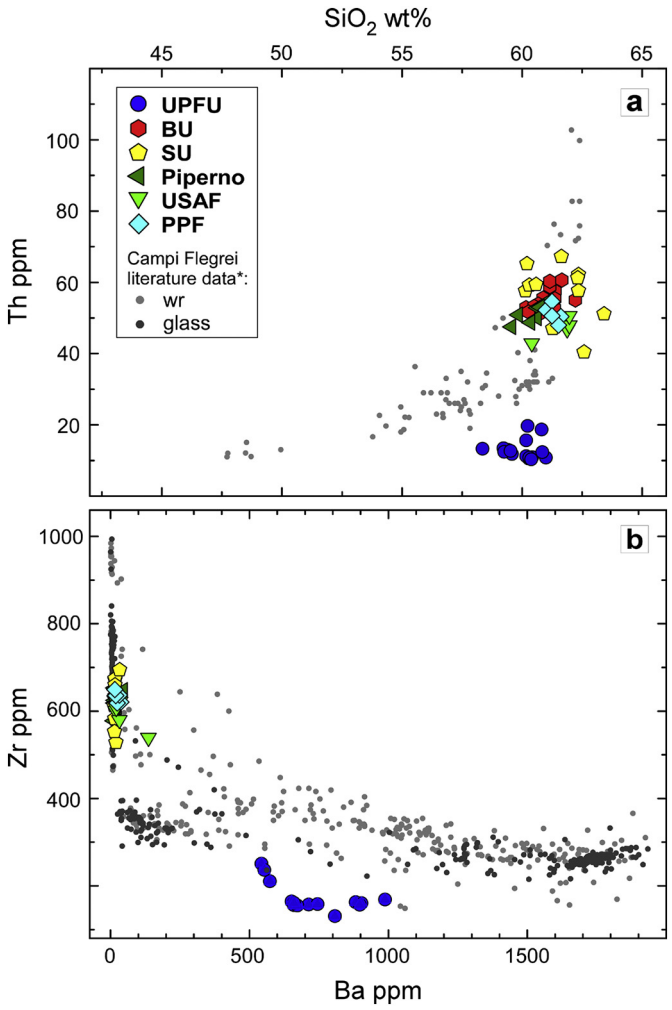

Fig. 7. Comparison between the composition of the San Martino glasses and the available literature data for whole-rocks (wr, light grey) and glasses (dark grey) of the Campi Flegrei volcanic field (data from GEOROC online database: http://georoc.mpch-mainz.gwdg.de/georoc/). Note that previous published data on the CI products are not plotted, but they generally overlap our data.

It worth noting that the Sr-Nd isotopic composition inferred for the incoming magma feeding the CI system falls slightly outside the whole-rock literature available for Campi Flegrei (Fig. 5b), plotting at lower $^{143}Nd/^{144}Nd$. These must represent an original characteristic of the incoming mafic melts, likely deriving from processes occurring in the mantle source of the magmas, which is not recorded in the whole-rock isotope composition of more evolved products. Interestingly, a recent study by Koornneef et al. (2015) on Italian K-rich magmas showed anomalously low $^{143}Nd/^{144}Nd$ in melt inclusions, which represent less evolved magmas in the systems than their host lavas. Although no data is available for the Campi Flegrei, their study do include Vesuvius volcano (Fig. 5b), which is close and compositionally similar to the Campi Flegrei. In all our calculations (Supplementary Table 6, Figs. 8,9) we considered an incoming mafic magma with $^{143}Nd/^{144}Nd$ equal to the lowest value measured in our dataset, but it cannot be excluded that the incoming magmas had even less radiogenic Nd isotopes. This would reduce the amount of mafic magma required to reproduce the composition of the erupted UPFU melts with respect to what discussed in the following section and reported in Figs. 8, 9 and 10.

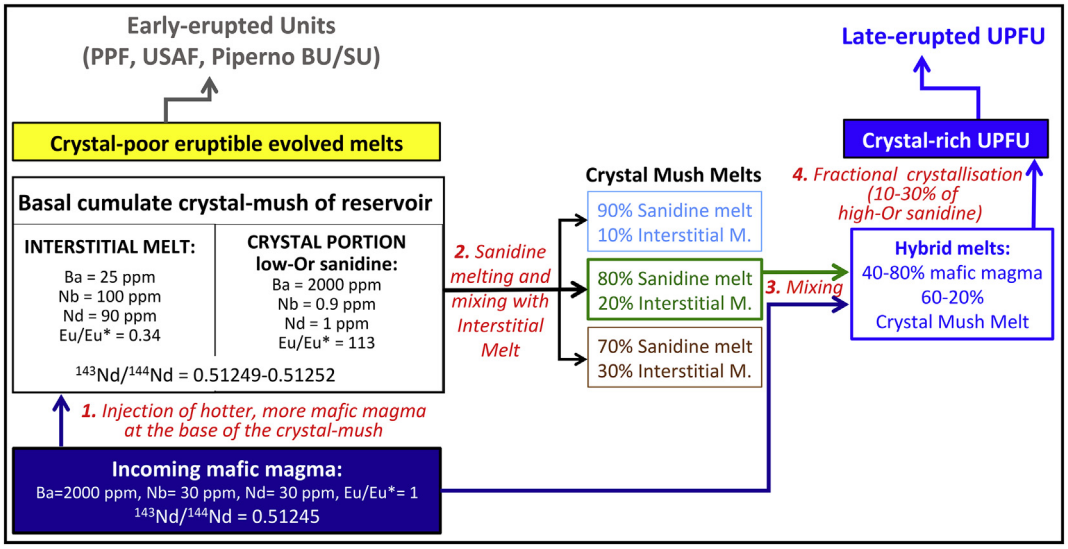

Fig. 8. Schematic summary of the compositions of the involved components and the processes (numbered in time order of occurrence) considered in the quantitative model for the UPFU magma formation, reported in Fig. 9. The abbreviations of the proximal-CI units are reported in Fig. 1.

5.2.2. Evidence for the contribution of the Crystal-Mush Melts

UPFU pyroclasts contain 25–30 vol% sanidine. Yet, the measured UPFU glasses do not show negative Eu/Eu* anomalies, but instead have Eu/Eu* ranging from unity up to 1.4 (Fig. 4). The high and variable Eu/Eu* values of UPFU glasses suggest a substantial role for the melting of feldspars (as also suggested by Forni et al., 2016, see also Wolff et al., 2020), which dominate the cumulate crystals of the crystal-mush. Indeed, it can be expected that the crystal-mush was constituted by the mineral phases directly segregated from the CI evolved magmas (low-Or sanidine, low-An plagioclase and low-Mg clinopyroxene (Fig. 2) and other minerals in clear geochemical disequilibrium with the evolved CI melts (high-An plagioclases and diopsidic clinopyroxenes) possibly representing antecrysts related to the previous Campi Flegrei volcanic activities (pre-CI eruptions). Any crystal-mush must also contain a certain amount (<40%; Marsh, 1981) of interstitial melt, which has to be involved in the UPFU magma generation. The key role of the interstitial melts in determining the isotopic composition of erupted magmas interacting with crystal-mushes has been also demonstrated for other systems (e.g., Stromboli, Bragagni et al., 2014).

In order to induce melting of feldspar crystals (mainly low-Or sanidine), the new input magma at the bottom of the reservoir crystal-mush had to be hotter and more mafic (hereafter "mafic magma") than the erupted UPFU melt. We suggest that, as they formed, the newly produced feldspar-melts mixed with the interstitial melt already present within the mush, thus forming a mixture, referred hereafter as "Crystal Mush Melt" (Fig. 8). As this process proceeded, the mush crystallinity decreased so that the mafic magma could have more easily migrated through the crystal-mush, then starting to mix with the Crystal Mush Melt.

We tried to reproduce the compositional variability of the UPFU by mixing an incoming mafic magma (assumed to be similar to the least radiogenic UPFU glasses, with Eu/Eu* = 1) and three possible Crystal Mush Melt compositions made up by different proportions of feldspar-melt and interstitial melt (Figs. 8,9a,b). The components and processes involved in the mixing model are summarized in Fig. 8 and the elemental and isotopic compositions of all the components used in the calculation are reported in Supplementary Table 6.

Based on the discussions above, the interstitial melt was assumed similar to the evolved magmas of the early-erupted units, which are interpreted to represent the eruptible melt-dominated part in the reservoir. Accordingly, we used the average trace element contents of glasses of the early-erupted units as representative of those of the interstitial melt. The Nd isotope composition of the interstitial melt was also considered equal to that of the early-erupted units. In order to account for the whole possible isotopic variation, we performed the calculation using the two extreme Nd-isotope values measured in the early-erupted units (Fig. 9a). The same isotopic range was used for the feldspar-melt, assuming that crystals and interstitial melt were in isotopic equilibrium within the crystal-mush.

The trace element composition of the feldspar-melt was calculated by assuming melting of only low-Or sanidine, since it represents the most abundant phase in the crystal-mush and also the first phase to be melted when the system is heated (Forni et al., 2016). Melting of low-An plagioclase cannot be excluded, but we did not include it in the mixing model, considering also that it is would be similar to low-Or sanidine in terms of Eu/Eu* positive anomalies, incompatible trace contents and Nd-isotopes. The starting composition of low-Or sanidine (Supplementary Table 6) was calculated assuming averaged trace element contents from literature data of sanidine from the CI (Fedele et al., 2015; Forni et al., 2016). Since feldspar melting degree could have been variable and related to the temperature reached by the surrounding interstitial melt and the relative melt volumes, we modelled two end-member scenarios to consider both partial (melt fraction F = 0.1) and whole (F = 1) melting of low-Or sanidine. Partition coefficients used for the melting calculation (Supplementary Table 6) were taken from literature on both the CI (Fedele et al., 2015; Forni et al., 2016) and other trachy-phonolitic rocks (Pappalardo et al., 2008; Villemant, 1988).

The calculated feldspar melts are characterised by high Eu/Eu*, but depleted in incompatible trace elements. On the contrary, the interstitial melt is extremely enriched in incompatible trace elements (including Nd) and has a strong Eu negative anomaly. Therefore, the relative proportions of these two different melt components in the Crystal Mush Melt are critical to reproduce the overall composition of the UPFU glasses.

Our calculations indicate that mixing a mafic magma with different amounts (up to about 60%) of a Crystal Mush Melt, made by about 20% of interstitial melt and 80% of low-Or sanidine-melt, can reproduce the UPFU incompatible element characteristics (mixing lines 2 and 3 of Fig. 9a,b), although not perfectly reproducing the combined $^{143}Nd/^{144}Nd$ and Eu/Eu*. Lower proportions of interstitial melt (10%; mixing lines 1 of Fig. 9a,b), do not sufficiently increase the $^{143}Nd/^{144}Nd$ values. Higher amounts of interstitial melt (e.g., 30%;

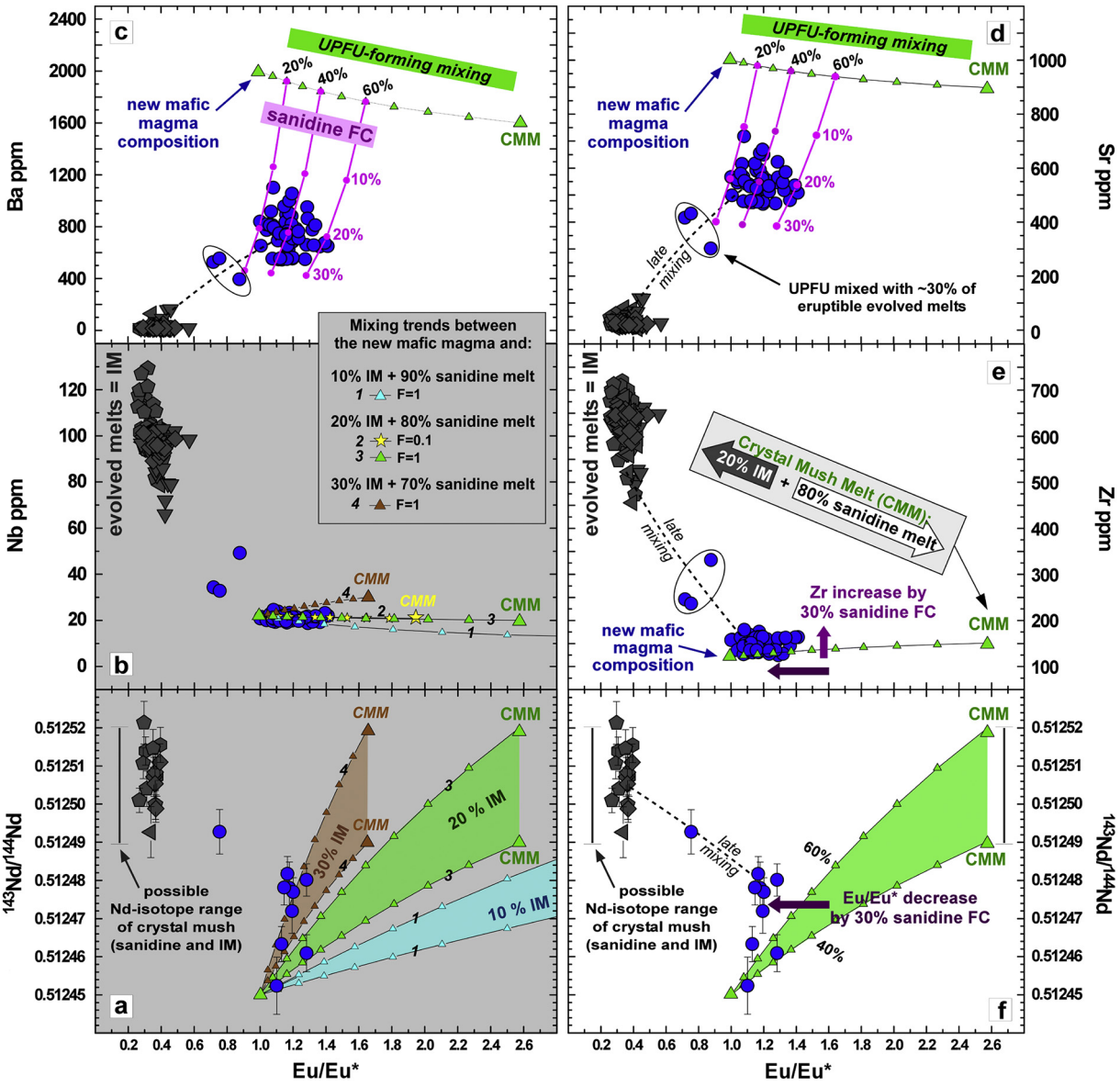

Fig. 9. Modeling of UPFU glasses evolution. The two plots with grey background (a, b) show modelled mixing processes between an incoming mafic magma and three different Crystal Mush Melts (CMM), made up by different proportion of sanidine-melts and interstitial melts (IM) (Fig. 8). In a) mixing models are made considering two extreme Nd-isotope values for the CMM. In b) the CMM mixture made of 80% sanidine melt +20% IM has been modelled considering both partial (melt fraction F = 0.1, curve 2) and bulk (F = 1, mixing curve 3) sanidine melting. In c), and d) the effect of contemporaneous fractional crystallization (FC) of sanidine (from 15 to 30%) is also modelled starting from various hybrid melts. In e) and f) the effect of fractional crystallization of 30% sanidine is represented by the dark purple arrows. Note that the effect of sanidine fractionation is able to explain the difference between the data and the mixing model in terms of Eu/Eu* and $^{143}Nd/^{144}Nd$ (f). The black dashed lines (c,d,e,f) defines the late magma mixing process between the eruptible evolved melts and the UPFU magmas. Symbols on UPFU-forming mixing lines represent 10% increments of CMM addition to the incoming mafic magma. The compositions of all the involved components and partition coefficients are reported in Fig. 8 and Supplementary Table 6.

mixing lines 4 of Fig. 9a,b) would fit better Eu anomalies and Nd-isotope ratios (Fig. 9a), but they would also produce an excessive enrichment in incompatible trace elements (Fig. 9b), which instead remain constant at relatively low contents in the UPFU glasses (Fig. 9b). Our model also indicates that whole sanidine melting (F = 1 in Fig. 9a,b) is more suitable than partial melting (F = 0.1). Sanidine melts produced at small degrees have lower Eu/Eu*, hence decreasing the Eu/Eu* of the Crystal Mush Melt (large yellow star in Fig. 9b). In this case, the incompatible trace element contents of UPFU would required a large amount of Crystal Mush Melt (up to 70%), which in turn would increase the Nd-isotope composition above the values measured in the UPFU glasses.

In summary, a Crystal Mush Melt made up by a mixture of 20% interstitial melt and 80% of whole sanidine-melt, seems to be the most suitable end-member to mix with the new mafic magma, although it still cannot perfectly reproduce the combined variation of $^{143}Nd/^{144}Nd$ and Eu/Eu*. In order to explain this, we must consider the possible additional role of fractional crystallization, which would affect Eu/Eu* as well as compatible trace elements. This will be discussed in the following sections 5.2.3 and 5.2.4.

5.2.3. Petrographic and mineralogical evidence for understanding the UPFU magma characteristics

The petrographic and mineral chemistry characteristics of the CI units provide further constraints on the origin of the UPFU magma. High-Or sanidine is almost uniquely found in the UPFU juveniles, with equilibrium textures and with no petrographic evidence of resorption.

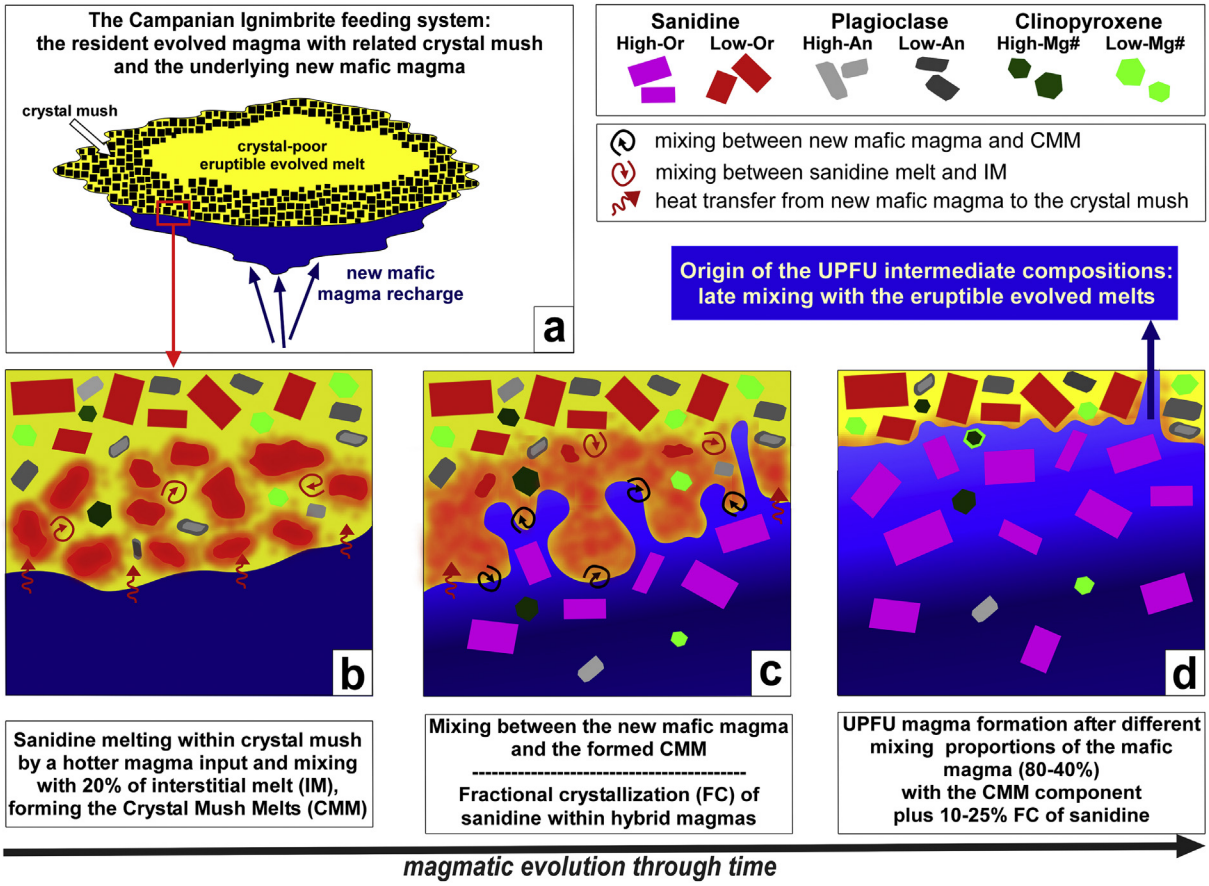

Fig. 10. Schematic cartoons for the UPFU magma formation after the reactivation of the CI crystal-mush by a new mafic magma. a) The CI magma chamber is represented by a crystal-mush model. The evolved trachy-phonolitic melts feeding most of the CI eruption (in yellow), represent the buoyant eruptible magma portion of the resident reservoir extracted from a cumulate crystal-mush zone during fractional crystallization. These melts fed all the crystal-poor units from the basal PPF to the *syn*-caldera BU/SU, through the USAF and Piperno units. b) The arrival of hotter mafic magmas (in blue) at the base of the CI reservoir allowed heating of the crystal-mush and its reactivation by whole melting of mainly low-Or sanidines. High-An plagioclases and high-Mg# clinopyroxenes were not affected by melting remaining as residual phases (Figs.8,9). c) The refilling mafic magma was directly involved in generating the UPFU melts, and did not only act as heat source to remobilize the cumulate mush. The variable geochemical and isotopic composition of UPFU melts were generated by mixing processes between the new mafic magma and a Crystal Mush Melt (CMM) made of 80% sanidine-melts and 20% of interstitial melts (IM) with a composition similar to that the CI late-erupted evolved units (Figs.8,9). Sanidine melting reduced the mush crystallinity allowing the mafic magma to migrate upwards and mix with the CMM component. d) This mixing (involving the 40–80% of the new mafic magma mixed with CMM) produced progressively cooler hybrid melts (represented by different shades of blue), which underwent variable degrees of fractional crystallization of mainly high-Or sanidine (10–25%). The presence of few more evolved UPFU glasses testify the persistence of evolved magmas in the final CI eruption phase. Some of them, having hybrid intermediate compositions, suggest a late mixing process between the already formed UPFU magmas and the resident eruptible crystal-poor evolved melts, possibly occurred shortly before the onset of the eruption. The UPFU magmas were erupted through fractures of the caldera collapse, which possibly occurred after the outpouring of the great volume of crystal-poor evolved melts.

Low-Or sanidine, usually euhedral and with normal zoning, is mainly found in the early-erupted units (Fig. 2a). These compositional and textural characteristics suggest that sanidine phenocrysts are generally equilibrium minerals in the respective CI magmas, reinforcing the idea that the crystal-mush was characterised by low-Or sanidines crystallized from the more evolved CI magmas.

In this view, the few low-Or sanidine found in the UPFU (Fig. 2) may represent relicts of the crystal-mush melting process. The same can be true for the sanidine crystals with low Sr-Ba cores (i.e. in equilibrium with an evolved magma) and high Sr-Ba rims found by Forni et al. (2016) in the UPFU. On the other hand, the subordinate proportion of these particular types of crystals in the UPFU, with respect to high-Or sanidine, indicates that most of the cumulate low-Or sanidine of the crystal-mush was completely consumed, as suggested by our geochemical calculation. Melting may also have involved low-An plagioclases (or low-An plagioclase rims) that were likely present in the crystal-mush, but are not preserved in UPFU (Fig. 2a).

UPFU products also contain anhedral high-An plagioclase and high-Mg# clinopyroxenes, the latter often present as core of strongly zoned crystals with Fe-richer rims, showing disequilibrium textures. These phases cannot have crystallized directly from the trachy-phonolitic UPFU magmas displaying low CaO (2–3 wt%) and MgO (0.6–1 wt%) contents, but must derive from more primitive magmas. Accordingly, they must represent either antecrysts present in the initial crystal-mush (i.e. from the pre-CI volcanic activity) or be derived from the mafic mixing end-member. We prefer the first hypothesis based on the following considerations: i) high-Ca plagioclases and high-Mg clinopyroxenes are also found in the early-erupted units; ii) previous data (Arienzo et al., 2009 and authors' unpublished data) indicate that these minerals are in isotopic disequilibrium with all the CI magmas.

5.2.4. Evidence for the contribution of crystal fractionation processes

The abundant occurrence of euhedral high-Or sanidines in UPFU indicates that these melts underwent significant sanidine fractionation following their generation by mixing. This explains the similar behaviour of Ba and Sr in the UPFU glasses (Fig. 9c,d) and also implies that the input mafic magma should have been characterised by higher contents in these compatible trace elements. In Fig. 9c–f we attempted to account for the effect of high-Or sanidine crystallization in the quantitative model described in section 5.2.2 (Fig. 8), assuming starting abundances of Ba and Sr (2000 ppm and 1000 ppm, respectively) based on published values reported for Campi Flegrei rocks with up to 4–5 wt%

of CaO (e.g., Di Renzo et al., 2011; Pappalardo et al., 1999, 2002a), when sanidine starts to crystallize.

Fig. 9c,d shows that Ba and Sr contents of UPFU glasses can be quantitatively modelled applying different percentages of high-Or sanidine fractionation (up to 25%) starting from the variable compositions of hybrid melts between the input mafic magma and the Crystal Mush Melt defined in section 5.2.2 (i.e., formed by 20% interstitial melt +80% sanidine melt). Such a process would also decrease the Eu/Eu* of the UPFU melt. Subordinate low-Mg clinopyroxenes and biotite might have also constituted the equilibrium mineral paragenesis of UPFU magmas (Fig. 2c) (Arienzo et al., 2009; Forni et al., 2016), hence reducing the MgO contents to the resulting UPFU magmas down to their relatively low values (Fig. 3). However, the role of such mafic phases in controlling Ba, Sr and Eu/Eu* is negligible and thus was not considered in the model. Our calculations indicate that the melts with the highest Eu/Eu* require high sanidine fractionation (20–25%) starting from hybrid magmas formed by the highest proportions (about 60%) of the Crystal Mush Melt (Fig. 9c,d). This suggests that significant amounts of high-Or sanidine crystallization occurred in response to the simultaneous cooling of the new mafic magma as the mixing process proceeded. Accordingly, the relative variation of Eu/Eu* with Ba and Sr (i.e., triangular shapes cluster of data points in Fig. 9c,d) is consistent with faster crystallization rates for hybrid UPFU magmas formed by higher proportions of the "cool" Crystal Mush Melt end-member. In this process, melts with similarly low Sr and Ba contents at different Eu/Eu* could be produced at the same time, possibly just before the eruption, considering that the longer time required for greater mixing proportions was counterbalanced by faster crystallization rates and vice versa.

The effect of high-Or sanidine fractionation on Eu/Eu* helps to also explain the position of the UPFU glasses in the $^{143}Nd/^{144}Nd$ versus Eu/Eu* plot (Fig. 9f). In this diagram high-Or sanidine crystallization would shift the data horizontally toward lower Eu/Eu*, starting from the variable Nd-isotope compositions of the hybrid UPFU magma. The same process described above also explains the broadly vertical variation of $^{143}Nd/^{144}Nd$. Magmas with higher Nd-isotopes require greater hybridization with Crystal Mush Melt component, which in turn promoted larger sanidine fractionation and consequent decreasing of the Eu anomaly.

Incompatible elements, on the contrary, are little affected by this process (vertical arrow in Fig. 9e), maintaining low and constant contents in the measured glasses. In general, the incompatible trace element contents of the UPFU glasses are anomalously low when compared to typical values of trachy-phonolitic magmas of Campi Flegrei (Fig. 7). This is explained by the peculiar process responsible for the genesis of the UPFU magmas, where these elements are buffered to values similar to those of the input mafic magma due to the dilution effect of the large amount of low-Or sanidine melt (80%) in the Crystal Mush Melt.

The interpretation of the genesis of the crystal-rich UPFU magmas, based on the model described above (Figs. 8,9) is summarized in the cartoons of Fig. 10. It is important to stress that the amount of interstitial melt within the Crystal Mush Melt arising from our calculation (20%) is critical and puts important constraints on the actual amount of residual melts in the crystal-mush at the base of the CI reservoir. Indeed, lower or higher amounts of this melt would not allow to reproduce the composition of UPFU glasses in terms of Nd-isotopes and incompatible element contents (and Eu/Eu*), respectively.

5.3. Origin of the more evolved UPFU compositions

A few of the measured UPFU glasses have compositions that are more evolved than those typical of this unit. These can be further divided in two groups: i) glasses with compositions similar to those of the early-erupted units (Figs. 3a,5), ii) glasses with intermediate compositions (Figs. 3–6) plotting on a straight line between the two melts in inter-elemental diagrams (Fig. 3).

The first group, only found in light pumiceous clasts, can be interpreted as melts that were derived from the main volume of eruptible melt (early-erupted units), but that remained in the reservoir and were not discharged until the end of the eruption, when mingled with the less evolved hybrid melts of UPFU.

The second group can be interpreted as melts formed by mixing and homogenisation of the early-erupted melts and UPFU magma (Fig. 9c–f), as evident also from the linear trends shown in Fig. 3. This late mixing process was possibly favoured by the consumption of the rigid crystal-mush during the formation of the UPFU magma, which allowed it to come in contact with the eruptible portion of the reservoir (Fig. 10d).

6. Conclusive remarks

We performed a detailed micro-analytical study on glasses and minerals of juvenile components from proximal-CI deposits, sampled in the most complete stratigraphic sequence of San Martino.

The data indicate that the eruption was fed by two distinct melts without the existence of a vertical geochemical gradient along the stratigraphy that was instead suggested on the basis of whole-rock analyses (Fedele et al., 2016; Forni et al., 2016; Melluso et al., 1995; Pappalardo et al., 2002b).

Evolved trachy-phonolitic melts fed most of the CI eruption emplacing the crystal-poor units from the basal PPF to the *syn*-caldera BU/SU, through the USAF and Piperno. We interpret the CI magma chamber in terms of a crystal-mush system, in agreement with Forni et al. (2016), where these evolved melts represent the buoyant eruptible magma portion of the CI reservoir, extracted from a cumulate crystal-mush zone during fractional crystallization.

A marked compositional change occurs in the juveniles of the topmost crystal-rich UPFU deposit of the proximal-CI, erupted just after the caldera collapse. These are sanidine-rich black scoriae, hosting less evolved (yet still trachy-phonolitic) glasses with distinctive compositions (also compared with the other Campi Flegrei trachy-phonolites), namely, i) higher and variable Sr and Ba contents, ii) lower and homogeneous incompatible element abundances, iii) high Eu/Eu* between 1.0 and 1.4, iv) variable and lower $^{143}Nd/^{144}Nd$ values. The UPFU magmas resided at the base of the CI reservoir (possibly sited at 7–8 km depth, Zollo et al., 2008) at the time of eruption and were finally erupted thanks to the caldera collapse fractures (Fedele et al., 2016). The existence of two isotopically distinct CI magmas was also suggested by Arienzo et al. (2009, 2011), based on the isotopic composition of medial-CI deposits; our UPFU Nd-isotope data reach even lower values (up to 0.51245) than those previously reported, reinforcing the idea that so low Nd-radiogenic magmas were never erupted at Campi Flegrei prior to the CI (Arienzo et al., 2009).

Quantitative calculations indicate that the unique composition of the UPFU melts derived from multiple evolutionary processes occurring when new mafic magmas reactivated the CI crystal-mush, physically interacting with it (Fig. 10). The arrival of hotter mafic magmas at the base of the CI reservoir allowed heating and reactivation of the crystal-mush by melting of low-Or sanidine (and minor low-An plagioclase) (Fig. 10a,b). A similar process was suggested by Forni et al. (2016), but our evidence further show that sanidine underwent whole rather than partial melting and that the high-An plagioclases (and high-Mg# clinopyroxenes) represented residual phases not affected by crystal-mush melting rather than minerals derived from the recharging mafic magmas. In addition, the low $^{143}Nd/^{144}Nd$ of UPFU glasses demonstrate that the refilling mafic magma was directly involved in generating the UPFU melts, and did not only act as heat source to remobilize the cumulate mush as proposed by Forni et al. (2016). The variable geochemical and isotopic composition of UPFU glasses can be reproduced with variable proportions (40–80%) of the new mafic magma mixed with a Crystal Mush Melt made of 80% sanidine-melts

and 20% of the original interstitial melts having a similar composition to the CI evolved units (Figs. 8–10). The calculated amount of mafic magma involved in the genesis of UPFU may be slightly overestimated considering that the incoming melts could have lower $^{143}Nd/^{144}Nd$ than that used in the calculation. On the other hand, we infer that the calculated 20% value may represent the actual proportion of interstitial melt within the CI crystal-mush.

Melting of sanidine reduced the mush crystallinity allowing the mafic magma to migrate upwards and mix with the Crystal Mush Melt component in variable proportions (60–20%). Such mixing produced progressively cooler hybrid melts that underwent variable degrees (10–25%) of fractional crystallization of mainly high-Or sanidine, depending on the time and/or the extent of mafic melt hybridization and then cooling (Figs. 9c–f, 10c,d).

The presence of few more evolved UPFU glasses testify the persistence of evolved magmas in the final CI eruption phase. Some of them have hybrid compositions showing a late mixing between the UPFU melts and the resident crystal-poor ones, possibly occurred a short time before the eruption (Figs. 9,10d). To allow the physical interaction between the two magmas, we speculate that most of the rigid crystal-mush present at the bottom of the CI reservoir was reactivated by the mafic input and transformed in the UPFU magmas. At the same time, the incoming magma was largely modified by the interaction with the Crystal Mush Melt component, explaining why mafic glass compositions are not found in the erupted products.

As for the volumes/masses involved in this process, it is noteworthy that UPFU is found in proximal-CI outcrops with reduced thickness indicating small magma volumes. However, similar compositions have been found both in medial (Arienzo et al., 2009; Civetta et al., 1997; Tomlinson et al., 2012) and distal (Lowe et al., 2012) CI outcrops, suggesting that the erupted volumes of UPFU magma might be significant. Indeed, studies on distal deposits suggested that roughly half of the co-ignimbrite plume (with a total estimated volume of 60 km^3 DRE; Marti et al., 2016) may have been constituted by less evolved (UPFU-like) magmas (Lowe et al., 2012; Smith et al., 2016).

In summary, our detailed geochemical and isotopic study on matrix glasses from the proximal-CI outcrop of San Martino, adds key constraints to processes preceding the eruption of the CI. The data indicate that the arrival of new hot magmas triggered a series of extremely complex processes, including crystal melting, mixing and crystallization. Similar mechanisms can occur also in other systems where crystal-mushes are reactivated by new mafic magma inputs (e.g. Wolff et al., 2015, 2020).

Declaration of Competing Interest

The authors declare that they have no known competing financial interests or personal relationships that could have appeared to influence the work reported in this paper.

Acknowledgments

The authors wish to thank Eleonora Braschi and Andrea Orlando (IGG-CNR, sezione di Firenze, Italy) for the invaluable help with EMPA analyses and Maurizio Ulivi for his help during isotope measurements at Laboratori "F.Olmi", DST, Università degli Studi di Firenze (Italy). The authors warmly thank jean-Luc Devidal for his support during EMPA and LA-ICP-MS analyses at the Laboratoire Magmas et Volcans (Université Clermont Auvergne, France) and Francesco D'Assisi Tramparulo (INGV-sezione di Napoli) for his essential support during the sampling in the Campi Flegrei area. The manuscript was greatly improved by thoughtful comments by Francesca Forni and an anonymous reviewer. SDS was funded by a doctoral fellowship (Pegaso) at the Università degli Studi di Firenze, (Italy) and a financial support was also provided by Italian MIUR, through the PRIN2015 funding grant 2015EC98J5, issued to RA and PRIN2017 funding grant 20178LPCPW, issued to LF.

Appendix A. Supplementary data

Supplementary data to this article can be found online at https://doi.org/10.1016/j.lithos.2020.105780.

References

Arienzo, I., Civetta, L., Heumann, A., Wörner, G., Orsi, G., 2009. Isotopic evidence for open system processes within the Campania Ignimbrite (Campi Flegrei - Italy) magma chamber. Bull. Volcanol. 71, 285–300.

Arienzo, I., Heumann, A., Wörner, G., Civetta, L., Orsi, G., 2011. Processes and timescales of magma evolution prior to the Campanian Ignimbrite eruption (Campi Flegrei, Italy). Earth Planet. Sci. Lett. 306, 217–228.

Avanzinelli, R., Boari, E., Conticelli, S., Francalanci, L., Guarnieri, L., Perini, G., Petrone, C.M., Tommasini, S., Ulivi, M., 2005. High precision Sr, Nd, and Pb isotopic analyses using the new generation thermal Ionisation mass spectrometer thermofinnigan triton-Ti®. Period. Mineral. 74 (3), 147–166.

Bachmann, O., 2010. The petrologic evolution and pre-eruptive conditions of the rhyolitic Kos Plateau Tuff (Aegean arc). Open Geosci. 2 (3), 270–305.

Bachmann, O., Bergantz, G.W., 2008. Rhyolites and their source mushes across tectonic settings. J. Petrol. 49 (12), 2277–2285.

Bachmann, O., Huber, C., 2016. Silicic magma reservoirs in the Earth's crust. Am. Mineral. 101 (11), 2377–2404.

Bachmann, O., Deering, C.D., Lipman, P.W., Plummer, C., 2014. Building zoned ignimbrites by recycling silicic cumulates: insight from the 1,000 km(3) Carpenter Ridge Tuff, CO. Contrib. Mineral. Petrol. 167 (6).

Bacon, C.R., Druitt, T.H., 1988. Compositional evolution of the zoned calcalkaline magma chamber of Mount Mazama, Crater Lake, Oregon. Contrib. Mineral. Petrol. 98 (2), 224–256.

Barberi, F., Innocenti, F., Lirer, L., Munno, R., Pescatore, T.S., Santacroce, R., 1978. The Campanian Ignimbrite: a major prehistoric eruption in the neapolitan area (Italy). Bull. Volcanol. 41, 10–22.

Bragagni, A., Avanzinelli, R., Freymuth, H., Francalanci, L., 2014. Recycling of crystal mush-derived melts and short magma residence times revealed by U-series disequilibria at Stromboli volcano. Earth Planet. Sci. Lett. 404, 206–219.

Cappelletti, P., Cerri, G., Colella, A., de'gennaro, M., Langella, A., Perrotta, A., Scarpati, C., 2003. Post-eruptive processes in the Campanian Ignimbrite. Mineral. Petrol. 79, 79–97.

Cashman, K.V., Giordano, G., 2014. Calderas and magma reservoirs. J. Volcanol. Geotherm. Res. 288, 28–45.

Cashman, K.V., Sparks, R.S.J., Blundy, J.D., 2017. Vertically extensive and unstable magmatic systems: a unified view of igneous processes. Science 355 (6331). https://doi.org/10.1126/science.aag3055.

Civetta, L., Carluccio, E., Innocenti, F., Sbrana, A., Taddeucci, G., 1991. Magma chamber evolution under the Phlegraean Fields during the last 10 ka: trace element and isotope data. Eur. J. Mineral. 3, 415–428.

Civetta, L., Orsi, G., Pappalardo, L., Fisher, R.V., Heiken, G., Ort, M., 1997. Geochemical zoning, mingling, eruptive dynamics and depositional processes - the Campanian Ignimbrite, Campi Flegrei caldera, Italy. J. Volcanol. Geotherm. Res. 75, 183–219.

Cooper, G.F., Wilson, C.J., Millet, M.A., Baker, J.A., Smith, E.G., 2012. Systematic tapping of independent magma chambers during the 1 Ma Kidnappers supereruption. Earth Planet. Sci. Lett. 313, 23–33.

Costa, A., Folch, A., Macedonio, G., Giaccio, B., Isaia, R., Smith, V.C., 2012. Quantifying volcanic ash dispersal and impact of the Campanian Ignimbrite super-eruption. Geophys. Res. Lett. 39, L10310.

D'Antonio, M., Civetta, L., Orsi, G., Pappalardo, L., Piochi, M., Carandente, A., De Vita, S., Di Vito, M.A., Isaia, R., 1999. The present state of the magmatic system of the Campi Flegrei caldera based on a reconstruction of its behavior in the past 12 ka. J. Volcanol. Geotherm. Res. 91, 247–268.

D'Antonio, M., Tonarini, S., Arienzo, I., Civetta, L., Di Renzo, V., 2007. Components and processes in the magma genesis of the Phlegrean Volcanic District, Southern Italy. Spec. Pap. Geol. Soc. Am. 418, 203–220.

Di Renzo, V., Arienzo, I., Civetta, L., D'Antonio, M., Tonarini, S., Di Vito, M.A., Orsi, G., 2011. The magmatic feeding system of the Campi Flegrei caldera: architecture and temporal evolution. Chem. Geol. 281 (3–4), 227–241.

Di Vito, M.A., Arienzo, I., Braia, G., Civetta, L., D'Antonio, M., Di Renzo, V., Orsi, G., 2011. The Averno 2 fissure eruption: a recent small-size explosive event at the Campi Flegrei Caldera (Italy). Bull. Volcanol. 73, 295–320.

Fedele, F.G., Giaccio, B., Isaia, R., Orsi, G., 2002. Ecosystem Impact of the Campanian Ignimbrite Eruption in late Pleistocene Europe. Quat. Res. 57, 420–424.

Fedele, L., Scarpati, C., Lanphere, M., Melluso, L., Morra, V., Perrotta, A., Ricci, G., 2008. The Breccia Museo formation, Campi Flegrei, southern Italy: geochronology, chemostratigraphy and relationship with the Campanian Ignimbrite eruption. Bull. Volcanol. 70, 1189–1219.

Fedele, L., Zanetti, A., Morra, V., Lustrino, M., Melluso, L., Vannucci, R., 2009. Clinopyroxene/liquid trace element partitioning in natural trachyte–trachyphonolite systems: insights from Campi Flegrei (southern Italy). Contrib. Mineral. Petrol. 158 (3), 337–356.

Fedele, L., Lustrino, M., Melluso, L., Morra, V., Zanetti, A., Vannucci, R., 2015. Trace-element partitioning between plagioclase, alkali feldspar, Ti-magnetite, biotite, apatite, and

evolved potassic liquids from Campi Flegrei (Southern Italy). Am. Mineral. 100 (1), 233–249.
Fedele, L., Scarpati, C., Sparice, D., Perrotta, A., Laiena, F., 2016. A chemostratigraphic study of the Campanian ignimbrite eruption (Campi Flegrei, Italy): insights on magma chamber withdrawal and deposit accumulation as revealed by compositionally zoned stratigraphic and facies framework. J. Volcanol. Geotherm. Res. 324, 105–117.
Fisher, R.V., Orsi, G., Ort, M., Heiken, G., 1993. Mobility of a large-volume pyroclastic flow—emplacement of the Campanian ignimbrite, Italy. J. Volcanol. Geotherm. Res. 56 (3), 205–220.
Foley, M.L., Miller, C.F., Gualda, G.A.R., 2020. Architecture of a super-sized magma chamber and remobilization of its basal cumulate (Peach Spring Tuff, USA). J. Petrol. https://doi.org/10.1093/petrology/egaa020.
Forni, F., Bachman, O., Mollo, S., De Astis, G., Gelmand, S.G., Ellisa, B.S., 2016. The origin of a zoned ignimbrite: Insights into the Campanian Ignimbrite magma chamber (Campi Flegrei, Italy). Earth Planet. Sci. Lett. 449, 259–271.
Fowler, S.J., Spera, F.J., Bohrson, W.A., Belkin, H.E., De Vivo, B., 2007. Phase equilibria constraints on the chemical and physical evolution of the Campanian Ignimbrite. J. Petrol. 48, 459–493.
Gebauer, S.K., Schmitt, A.K., Pappalardo, L., Stockli, D.F., Lovera, O.M., 2014. Crystallization and eruption ages of Breccia Museo (Campi Flegrei caldera, Italy) plutonic clasts and their relation to the Campanian ignimbrite. Contrib. Mineral. Petrol. 167, 1–18.
Giaccio, B., Isaia, R., Fedele, F.G., Di Canzio, E., Hoffecker, J., Ronchitelli, A., Sinitsyn, A.A., Anikovich, M., Lisitsyn, S.N., Popov, V.V., 2008. The Campanian Ignimbrite and Codola tephra layers: two temporal/stratigraphic markers for the early Upper Palaeolithic in southern Italy and eastern Europe. J. Volcanol. Geotherm. Res. 177, 208–226.
Giaccio, B., Hajdas, I., Isaia, R., Deino, A., Nomade, S., 2017. High-precision 14C and 40Ar/39Ar dating of the Campanian Ignimbrite (Y-5) reconciles the time-scales of climatic-cultural processes at 40 ka. Sci. Rep. 7, 45940.
Gualda, G.A., Ghiorso, M.S., 2013. Low-pressure origin of high-silica rhyolites and granites. J. Geol. 121 (5), 537–545.
Koornneef, J.M., Nikogosian, I., van Bergen, M.J., Smeets, R., Bouman, C., Davies, G.R., 2015. TIMS analysis of Sr and Nd isotopes in melt inclusions from Italian potassium-rich lavas using prototype 10^13 Ω amplifiers. Chem. Geol. 397, 14–23.
Le Maitre, R.W., Sabine, P.J., 1989. A classification of igneous rocks and glossary of Terms: recommendations of theinternational union of geological sciences subcommission on the systematics of igneous rocks. In: Bateman, P., Dudek, A., Keller, J., Lameyr, J., Le Bas, M.J., Schmidt, R., Zanettin, B. (Eds.), Blackwell Scientific Publications. Trowbridge, Wilts, England, pp. 1–193.
Lowe, J.J., Barton, N., Blockley, S., Ramsey, C.B., Cullen, V.L., Davies, W., Gamble, C., Grant, K., Hardiman, M., Housley, R., Lane, C.S., Lee, S., Lewis, M., MacLeod, A., Menzies, M.A., Muller, W., Pollard, M., Price, C., Roberts, A.P., Rohling, E.J., Satow, C., Smith, V.C., Stringer, C.B., Tomlinson, E.L., White, D., 2012. Volcanic ash layers illuminate the resilience of Neanderthals and early modern humans to natural hazards. Proc. Natl. Acad. Sci. U. S. A. 109, 13532–13537.
Marianelli, P., Sbrana, A., Proto, M., 2006. Magma chamber of the Campi Flegrei supervolcano at the time of eruption of the Campanian Ignimbrite. Geology 34 (11), 937–940.
Marsh, B.D., 1981. On the crystallinity, probability of occurrence, and rheology of lava and magma. Contrib. Mineral. Petrol. 78 (1), 85–98.
Marti, A., Folch, A., Costa, A., Engwell, S., 2016. Reconstructing the plinian and co- ignimbrite sources of large volcanic eruptions: a novel approach for the Campanian Ignimbrite. Sci. Rep. 1–11.
Melluso, L., Morra, V., Perrotta, A., Scarpati, C., Adabbo, M., 1995. The eruption of the Breccia Museo (Campi Flegrei, Italy): fractional crystallization processes in a shallow, zoned magma chamber and implications for the eruptive dynamics. J. Volcanol. Geotherm. Res. 68, 325–339.
Orsi, G., D'Antonio, M., De Vita, S., Gallo, G., 1992. The Neapolitan Yellow Tuff, a large-magnitude trachytic phreatoplinian eruption: eruptive dynamics, magma withdrawal and caldera collapse. J. Volcanol. Geotherm. Res. 53, 275–287.
Pabst, S., Wörner, G., Civetta, L., Tesoro, R., 2008. Magma chamber evolution prior to the Campanian Ignimbrite and Neapolitan Yellow Tuff eruptions (Campi Flegrei, Italy). Bull. Volcanol. 70, 961–976.
Pappalardo, L., Civetta, L., D'Antonio, M., Deino, A., Di Vito, M., Orsi, G., Carandente, A., de Vita, S., Isaia, R., Piochi, M., 1999. Chemical and Sr-isotopic evolution of the Phlegrean magmatic system before the Campanian Ignimbrite and the Neapolitan yellow tuff eruptions. J. Volcanol. Geotherm. Res. 91, 141–166.
Pappalardo, L., Piochi, M., D'Antonio, M., Civetta, L., Petrini, R., 2002a. Evidence for multi-stage magmatic evolution during the past 60 kyr at Campi Flegrei (Italy) deduced from Sr, Nd and Pb isotope data. J. Petrol. 43, 1415–1434.
Pappalardo, L., Civetta, L., de Vita, S., Di Vito, M., Orsi, G., Carandente, A., Fisher, R.V., 2002b. Timing of magma extraction during the Campanian Ignimbrite eruption (CampiFlegrei Caldera). J. Volcanol. Geotherm. Res. 114, 479–497.
Pappalardo, L., Ottolini, L., Mastrolorenzo, G., 2008. The Campanian Ignimbrite (southern Italy) geochemical zoning: insight on the generation of a super-eruption from catastrophic differentiation and fast withdrawal. Contrib. Mineral. Petrol. 156, 1–26.
Perrotta, A., Scarpati, C., Luongo, G., Morra, V., 2006. The Campi flegrei caldera boundary in the city of Naples. In: De Vivo, B. (Ed.), Volcanism in the Campania Plain: Vesuvius, Campi Flegrei and Ignimbrites 9. Elsevier, Amsterdam, pp. 85–96.
Pyle, D.M., Ricketts, G.D., Margari, V., van Andel, T.H., Sinitsyn, A.A., Praslov, N.D., Lisitsyn, S., 2006. Wide dispersal and deposition of distal tephra during the Pleistocene Campanian Ignimbrite/Y5 eruption, Italy. Quat. Sci. Rev. 25 (21−22), 2713–2728.
Rolandi, G., Bellucci, F., Heizler, M.T., Belkin, H.E., De Vivo, B., 2003. Tectonic controls on the genesis of ignimbrites from the Campanian Volcanic Zone, southern Italy. Mineral. Petrol. 79, 3–31.
Rosi, M., Vezzoli, L., Aleotti, P., De Censi, M., 1996. Interaction between caldera collapse and eruptive dynamics during the Campanian Ignimbrite eruption, Phlegraean Fields, Italy. Bull. Volcanol. 57 (7), 541–554.
Scarpati, C., Perrotta, A., 2016. Stratigraphy and physical parameters of the Plinian phaseof the Campanian Ignimbrite eruption. Geol. Soc. Am. Bull. 128 (7–8), 1147–1159.
Scarpati, C., Sparice, D., Perrotta, A., 2014. A crystal concentration method for calculating ignimbrite volume from distal ash-fall deposits and a reappraisal of the magnitude of the Campanian Ignimbrite. J. Volcanol. Geotherm. Res. 280, 67–75.
Signorelli, S., Vaggelli, G., Francalanci, L., Rosi, M., 1999. Origin of magmas feeding the Plinian phase of the Campanian Ignimbrite eruption, Phlegrean Fields (Italy): constraints based on matrix-glass and glass-inclusion compositions. J. Volcanol. Geotherm. Res. 91 (2–4), 199–220.
Smith, V.C., Isaia, R., Engwell, S.L., Albert, P.G., 2016. Tephra dispersal during the Campanian Ignimbrite (Italy) eruption: implications for ultra-distal ash transport during the large caldera-forming eruption. Bull. Volcanol. 78 (6), 45.
Thirlwall, M.F., 1991. Long-term reproducibility of multicollector Sr and Nd isotope ratio analysis. Chem. Geol. 94, 85–104.
Tomlinson, E.L., Arienzo, I., Civetta, L., Wulf, S., Smith, V.C., Hardiman, M., Lane, C.S., Carandente, A., Orsi, G., Rosi, M., Müller, W., Menzies, M.A., 2012. Geochemistry of the Phlegraean Fields (Italy) proximal sources for major Mediterranean tephras: implications for the dispersal of Plinian and co-ignimbritic components of explosive eruptions. Geochim. Cosmochim. Acta 93, 102–128.
Tonarini, S., D'Antonio, M., Di Vito, M.A., Orsi, G., Caradente, A., 2009. Geochemical and B-Sr-Nd isotopic evidence for mingling and mixing processes in the magmatic system that fed the Astroni Volcano (4.1-3.8 Ka) within the Campi Flegrei Caldera (Southern Italy). Lithos 107, 135–151.
Villemant, B., 1988. Trace element evolution in the Phlegrean Fields (Central Italy): fractional crystallization and selective enrichment. Contrib. Mineral. Petrol. 98 (2), 169–183.
Vitale, S., Isaia, R., 2014. Fractures and faults in volcanic rocks (Campi Flegrei, southern Italy): insight into volcano-tectonic processes. Int. J. Earth Sci. 103 (3), 801–819.
Voloschina, M., Pistolesi, M., Bertagnini, A., Métrich, N., Pompilio, M., Di Roberto, A., Di Salvo, S., Francalanci, L., Isaia, R., Cioni, R., Romano, C., 2018. Magmatic reactivation of the Campi Flegrei volcanic system: insights from the Baia–Fondi di Baia eruption. Bull. Volcanol. 80 (10), 75.
Wolff, J.A., Ellis, B.S., Ramos, F.C., Starkel, W.A., Boroughs, S., Olin, P.H., Bachmann, O., 2015. Remelting of cumulates as a process for producing chemical zoning in silicic tuffs: a comparison of cool, wet and hot, dry rhyolitic magma systems. Lithos 236-237, 275–286.
Wolff, J.A., Forni, F., Ellis, B.S., Szymanowski, D., 2020. Europium and barium enrichments in compositionally zoned felsic tuffs: a smoking gun for the origin of chemical and physical gradients by cumulate melting. Earth Planet. Sci. Lett. 540, 116251.
Zollo, A., Maercklin, N., Vassallo, M., Dello Iacono, D., Virieux, J., Gasparini, P., 2008. Seismic reflections reveal a massive melt layer feeding Campi Flegrei caldera. Geophys. Res. Lett. 25 (18).